Indian Journal of Pure & Applied Physics
Vol. 57, March 2019, pp. 196-204

Significance of HOMO and LUMO studies on dye doped glycene lithium sulphate (GLS) crystals for non-linear optical applications

G Suresh[a], K Sahadevan[a], K Sambathkumar[b]* & P Kumaresan[a]

[a] PG & Research Department of Physics , Thiru A Govindasamy Government Arts College, Tindivanam 604 002, India

[b] PG & Research Department of Physics, Arignar Anna Government Arts College, Villupuram 605 602, India

Received 13 December 2016; accepted 22 October 2018

The ideal material that could have potential applications in non-linear optical (NLO) devices should possess the combination of large non-linear figure of merit for frequency conversion, high laser damage threshold, fast optical response time, wide phase matchable angle, architectural flexibility for molecular design and morphology, optical transparency and high mechanical strength. The stability of glycene lithium sulphate (GLS) single crystal has been improved by doping organic dyes. The structural, chemical, optical, mechanical and non-linear optical properties of the dye doped crystals have been analyzed with the characterization studies such as powder XRD, FT-IR, UV-Visible and SHG measurements, respectively. NMR, HOMO and LUMO energies have been performed by time dependent density functional theory (TD-DFT) approach. The Mulliken charge analysis indicates that the sulphur atoms of the benzene ring and the OH group attached to the ring are the main reactive centers of glycene lithium sulphate. And the temperature dependence of the thermodynamic properties of constant pressure (C_p), entropy (S) and enthalpy change ($\Delta H0 \rightarrow T$) for glycene lithium sulphate have also been determined.

Keywords: GLS crystals, XRD studies, FT-IR, SHG measurements, HOMO–LUMO studies

1 Introduction

A nonlinear optical material has many applications like image application using photorefractive crystals, frequency multipliers and mixers, fiber optics, parameter oscillators, optical switches, *etc.*, laser in a modern wonder, whether it is in the field of information transformation or in the field of medicine[1-5]. The interaction of laser with matter has advanced capabilities in optical spectroscopy. The discovery of laser itself is a result of crystal growth[6-8]. In recent years more 0emphasis is given to semiorganic materials due to their much matured NLO applications than organic materials and owing to their good transparency, chemical stability, and mechanical properties. The large nonlinearity arises from the strong charge transfer and high polarisibility[9-11]. To enable a material to be potentially useful for NLO applications the material should be available in bulk single crystal form. Also research into the growth of large single crystals from aqueous solution is currently serving as the important avenue to general progress in understanding many fundamental concepts of crystallization. To understand the kinetics and mechanisms involved in the process of crystal growth, many theories such as surface energy theory, diffusion theory, surface adsorption theory, *etc.*, have been proposed. The first theory of crystal growth was proposed as early as the late 19th century. The development of the theories of crystal growth has thrown more light on the understanding of crystal growth phenomena. Compared with inorganic NLO materials, organic materials may fulfill many of these requirements, but there are also some drawbacks with organic NLO materials such as environmental stability, poor chemical and mechanical stability, red-shift of the cut-off wavelength, low laser damage thresholds and poor phase matching properties[12-14]. In order to overcome these drawbacks and improve the properties, the growth of semi-organic crystals has nowadays come into prominence. The semi organic crystals have some advantages such as higher second order optical non-linearities, short transparency cut-off wavelength and stable physio-chemical performance over the traditional inorganic and organic crystals[15]. For greater second harmonic generation (SHG) efficiency, one requires highly polarizable molecular system having asymmetric charge distribution in the molecule[16]. Since there is a

*Corresponding author (E-mail: sa975kumar@gmail.com)

large demand for crystals because of the revolution in electronic industries, it is required to synthesize new NLO materials and improve the properties of the existing materials. Considering all the above mentioned facts, glycene lithium sulphate crystals have been synthesized and grown moderately at low cost.

2 Experimental Procedure

2.1 Crystal growth

A solution of glycine lithium sulphate was prepared by dissolving equimolar amount of glycine and lithium sulphate. The solution was continuously stirrer using a magnetic stirrer of room temperature. The chemical reaction may be represented as:

$$C_2H_5NO_2 + Li_2SO_4 \rightarrow [Li_2(\ SO_4\ )(C_2H_5NO_2)]$$

The prepared solution was filtered and kept undisturbed in a constant temperature bath maintained at a temperature of 40 °C. When evaporation takes place slowly, super saturation is activated. As a result, crystals with dimensions 7.5 × 5 × 2.75 mm^3 were harvested in a period of 40 days. GLS crystals were grown from aqueous solution by slow evaporation method. The solubility of dyes doped GLS water was measured. It was found to be 16.5 g/100 ml at 40 ºC for coumarine doped GLS. The amount of GLS salt to be dissolved was determined from its solubility curve at an average temperature of 38 ºC. The solution was stirred long enough to ensure complete dissolution of the solute, and filtered. Subsequently the solution was cooled at a rate of 0.1 ºC/day. The seed crystals were prepared at low temperature by spontaneous nucleation (Fig.1 (a)). The seed crystals with perfect shape and free from macro defects were used for growth experiments. Seed crystals of pure GLS and doped GLS were grown using constant temperature bath controlled with an accuracy of ± 0.01 ºC. A supersaturated solution of coumarine doped GLS was prepared in distilled, deionized water. Seed crystals were introduced into the solution using thin nylon thread at the appropriate supersaturation condition. Experiments were allowed to run for considerably longer duration of the time (20 days) would grow large crystals.

3 Characterization Studies

3.1 Powder X-ray diffraction analysis

Powder X-ray diffraction studies were carried out for the as grown crystals using a Rich Seifert X-ray diffractometer with CuK_α (λ = 1.5405 Å) radiation (Kurtz 1968). Powder X-ray diffraction spectra of the grown crystals from pure and doped GLS are shown in Fig. 2. Powder XRD spectra for the pure and doped GLS revealed that the structures of the doped crystals were slightly distorted compared to the pure GLS crystal. The (*h*; *k*; *l*) planes satisfy the general reflection conditions of space group observed from the structure determination of the crystal. This may be attributed to strain on the lattice by the absorption or substitution of dye. It is observed that the reflection lines of the doped dye crystal correlate well with those observed in the individual parent compound with a slight shift in the Bragg angle.

3.2 FT-IR studies

The FT-IR spectra of pure and dye doped GLS crystals on a Bruker IFS 66V model spectrophotometer using 1064 nm output of a cw diode pumped Nd: YAG laser as a source of excitation in the region 500 – 4000 cm^{-1} operating at 200 mW power at the samples with a spectral resolution of 2 cm^{-1}. The observed FT-IR spectra of pure and doped GLS are shown in Fig. 3. In doped GLS spectra, broad peak around 3650 cm^{-1} was due to free –OH stretching vibration [17]. It reveals that at least one of the –OH group of GLS was remain unaltered after that doped with GLS. Due to the greater mass of sulphur in GLS the C=S stretching vibration was expected to occur at 625 cm^{-1}, it was considerably

Fig. 1 — Photograph of coumarine doped GLS crystal.

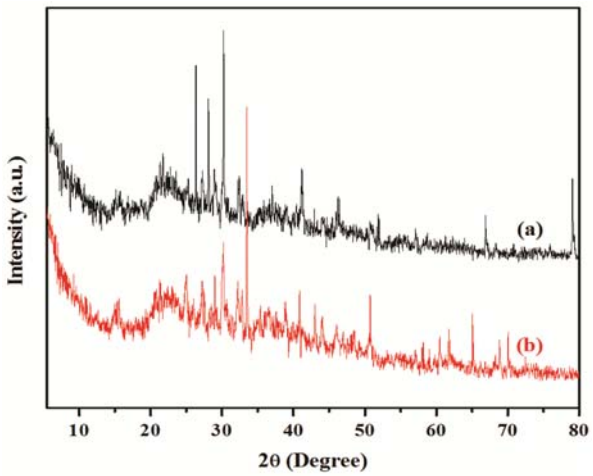

Fig. 2 — XRD spectra of (a) pure and (b) coumarine doped GLS crystal.

lower frequency than the usual C=O stretching vibration at 1710 cm^{-1} because of the C=S group is less polar than the C=O group and has a considerably weaker band. The strong vibrational coupling was operative in the case of nitrogen containing thiocarbonyl group of glycene and that the C=S vibration was not located in the spectra[18]. The comparison of FT-IR studies on pure and coumarine doped GLS crystals were given in Table 1.

3.3 UV-Visible studies

The transmission spectra were taken at room temperature using Varian Cary 2300 spectrometer (UV-VIS-NIR). The transmission spectra were recorded in the range 200-1200 nm for 1 mm thick c-cut plates of pure and coumarine doped GLS was shown in Fig. 4. All the crystals irrespective of the dopants are transparent in the entire visible region. The UV-Visible spectrum of Coumarine doped GLS crystal, maximum wavelength of absorption (λ_{max}) appeared at 780 cm^{-1}. Therefore, it reveals that after incorporation of coumarine dye, the UV absorption was shifted to Red region. The bathochromic shift (red shift) increases in accordance of mole fractions of dopants. The pure GLS crystal has about 75% of transmission. The dye doped GLS crystal is invariably has higher transmission percentage compared to pure GLS crystal. From the UV-Visible spectrum, transmission percentage increases due to addition of doped in GLS crystal, which would enhances the optical property of GLS crystal.

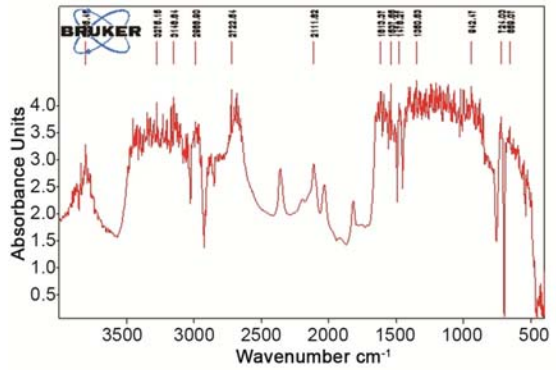

Fig. 3 — FT-IR spectrum of coumarine doped GLS crystal.

Table 1 — FT-IR Assignments of pure and coumarine doped GLS crystals.

Calculated frequency (cm^{-1})	Pure GLS	Coumarine doped GLS	Assignments
3615	3600(w)	3650(w)	Free O-H stretching
3200	-	3250(vw)	N-H asymmetric stretching
3100	3100(br)	-	Intramolecular H-bonded O-H stretching
2900	-	2900(br)	N-H symmetric stretching in NH_2 group
2650	2650(br)	-	O = P – OH asymmetric stretching of KDP
2250	2250(w)	2250(br)	P-O-H asymmetric stretching
1600	1650(br)	1650(vs)	O = P – OH symmetric stretching of KDP
1350	1300(sh)	1350(vs)	P=O symmetric stretching (aliphatic)
1150	1100(sh)	1150(vs)	P-O-H symmetric stretching
975	950(s)	-	O = P – OH bending
625	600(sh)	600(sh)	HO – P – OH bending

3.4 Microhardness studies

Microhardness is one of the important mechanical properties of the GLS crystals. It can be suitably used to measure the plastic properties and strength of a material. Microhardness measurements were carried out using Leitz Weitzler hardness tester fitted with a diamond indenter. The well-polished doped GLS crystal was placed on the platform of the Vickers micro hardness tester and the loads of different magnitudes (Fig. 4) were applied over a tester at a fixed interval of time. The indentation time was kept as 8 s for all the loads. The microhardness value was calculated using the relation $H_v = 1.8544 \times P/d^2$ kg/mm^2, where P is the applied load in kg and d is the diagonal length of the indentation impression in mm. Dye doping improves the mechanical strength of GLS. Microhardness values of doped GLS were tabulated in Table 2.

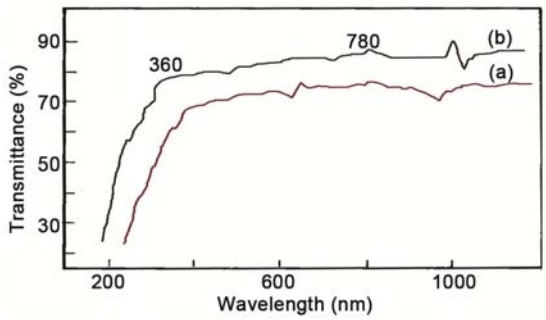

Fig. 4 — UV-Visible spectra of (a) pure GLS (b) coumarine doped GLS crystal.

Table 2 — Microhardness values of coumarine doped GLS crystals.

S No	Crystal	Micro hardness (kg/mm^2)
1	GLS	90.15
2	Coumarine doped GLS	101.56

3.5 Thermal studies

Figure 5 illustrates the differential thermal analysis (DTA) and thermo-gravimetric analysis (TGA) curves for the grown Coumarine doped GLS crystal. The DTA curve implies that the material undergoes an irreversible endothermic transition at 200 °C where the melting begins[18]. This peak was endothermic peak, represents the temperature at which the melting terminates which corresponds to its melting point at 210 °C. Ideally, the melting point of the trace corresponds to a vertical line. The sharpness of the endothermic peak shows good degree of crystallinity of the grown ingot. The exothermic peak at 290 °C indicates a phase change from liquid to vapour state as evident from the loss of weight of about 87% in TG curve[19].

3.6 NLO studies

The dye doped GLS crystals are used for the generation of second harmonics of Nd-based near-infrared solid-state lasers. The fundamental of an Nd:YAG laser (1064 nm) can be converted to 532 nm of second harmonic or its 355 nm of third harmonic or its 266 nm of fourth harmonic by using GLS crystals[20]. The performance of these frequency conversion devices can be seriously degraded if there are defect-associated absorption bands in the crystal which overlap the fundamental pump wavelength or one of the output wave lengths. Thus, it is important to identify and characterize all potentially harmful absorption bands in non-linear optical crystals. In order to confirm the suitability of the doped GLS crystal, the non-linear application, harmonic generation was tested using the Nd-YAG laser[21]. A small crystal was placed on the sample holder and the YAG laser beam was made to pass through the crystal and the output conversion of input as green light SHG was analyzed.

The efficiency of doped GLS crystals were compared with pure GLS and also show that dye doped GLS crystal has higher efficiency. A sample of GLS, also powdered was used for the same experiment as a reference material in the SHG measurement. It was found that the frequency doubling efficiency of the doped GLS is better than KDP[22]. A comparison of SHG property of GLS crystal with dye doped GLS crystal is presented in Table 3.

3.7 Frontier orbital energy

Many organic molecules that contain conjugated π electrons are characterized hyperpolarizabilities and

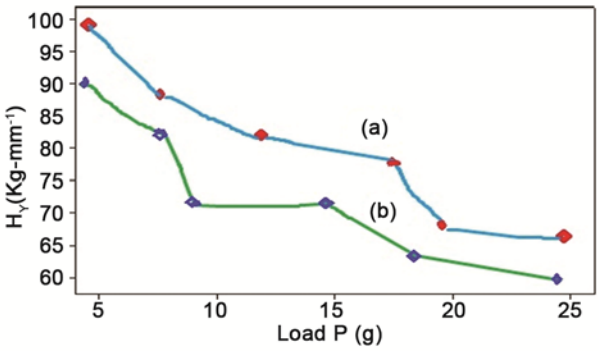

Fig. 5 — Microhardness studies of (a) coumarine doped GLS and (b) pure GLS crystals.

Table 3 — Comparison of SHG of pure and coumarine doped GLS crystals.

S No	Compound	SHG efficiency
1	KDP	1.00
2	Coumarine doped GLS crystals	1.65

are analyzed by means of vibrational spectroscopy. In most cases, even in the absence of inversion symmetry, the weakest bands in the Raman spectrum are strongest in the IR spectrum and vice versa. But the intra molecular charge transfer from the donor to accepter group through a single–double bond conjugated path can induce large variations of both the molecular dipole moment and the molecular polarizability, making IR and Raman activity strong at the same time. It is also observed in the title compound the bands in FTIR spectrum have their counterparts in Raman shows that the relative intensities in IR and Raman spectra are comparable resulting from the electron cloud movement through π conjugated frame work from electron donor to electron acceptor groups. Highest occupied molecular orbital (HOMO) and lowest unoccupied molecular orbital (LUMO) are very important parameters for quantum chemistry. Can determine the way the molecule interacts with other species; hence, they are called the frontier orbitals. HOMO, which can be thought the outermost orbital containing electrons, tends to give these electrons such as an electron donor. On the other hand; LUMO can be thought the innermost orbital containing free places to accept electrons[23]. Owing to the interaction between HOMO and LUMO orbital of a structure, transition state transition of π* type is observed with regard to the molecular orbital theory. Therefore, while the energy of the HOMO is directly related to the ionization potential, LUMO energy is directly related to the

electron affinity. Energy difference between HOMO and LUMO orbitals is called as energy gap that is an important stability for structures. In addition, the pictorial scheme of few MOs of Coumarin doped Glycene Lithium Sulphate is shown in Fig.6. HOMO is localized on the central ring and has partially contribution from the substitution groups such as oxygen and amino group. LUMO is quite localized on the central ring and has strong contribution from the substituted electronegative oxygen and S group. The energy gap between HOMO and LUMO is -0.1785 a.u., which shows that charge transfer may be taking place from the ring to oxygen atom. As seen from the Fig. 6, HOMO-1 is very similar to HOMO, rotated by 90°.

3.7.1 Global and local reactivity descriptors

Based on density functional descriptors global chemical reactivity descriptors of molecules such as hardness, chemical potential, softness, electronegativity and electrophilicity index as well as local reactivity have been defined[204]. Pauling introduced the concept of electronegativity as the power of an atom in a molecule to attract electrons to it. Hardness (η), chemical potential (μ) and electronegativity (χ) and softness are defined as:

$$\eta = \tfrac{1}{2}(\partial 2E/\partial N2)V(r) = \tfrac{1}{2}(\partial\mu/\partial N)V(r)$$
$$\mu = (\partial E/\partial N)V(r)$$
$$\chi = -\mu = -(\partial E/\partial N)V(r)$$

where E and $V(r)$ are electronic energy and external potential of an N-electron system respectively. Softness is a property of molecule that measures the extent of chemical reactivity. It is the reciprocal of hardness.

$$S = 1/\eta$$

Using Koopman's theorem for closed-shell molecules, η, μ and χ can be defined as:

$$\eta = (I - A)/2$$
$$\mu = -(I + A)/2$$
$$\chi = (I + A)/2$$

where A and I are the ionization potential and electron affinity of the molecules, respectively. The ionization energy and electron affinity can be expressed through HOMO and LUMO orbital energies as $I = -E_{HOMO}$ and $A = -E_{LUMO}$. Electron affinity refers to the capability of a ligand to accept precisely one electron from a donor. However in many kinds of bonding, *viz.*, covalent hydrogen bonding, partial charge transfer takes places. The new descriptor to quantify the global electrophilic power of the molecule as electrophilicity index (ω), which defines a quantitative classification of the global electrophilic nature of a molecule have proposed electrophilicity index (ω) as a measure of energy lowering due to maximal electron flow between donor and acceptor.

They defined electrophilicity index (ω) as follows:

$$\omega = \mu^2/2\,\eta$$

The usefulness of this new reactivity quantity has been recently demonstrated in understanding the toxicity of various pollutants in terms of their reactivity and site selectivity. The calculated value of electrophilicity index describes the biological activity of Coumarin doped Glycene Lithium Sulphate. All the calculated values of hardness, potential, softness and electrophilicity index are shown in Table 4.

3.8 Temperature dependence of thermodynamic properties

The temperature dependence of the thermodynamic properties heat capacity at constant pressure (Cp), entropy (S) and enthalpy change ($\Delta H0 \rightarrow T$) for Coumarin doped glycene lithium sulphate were also

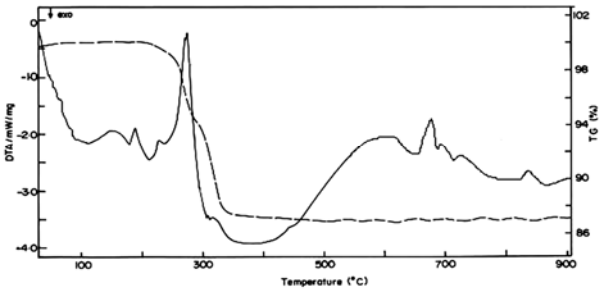

Fig. 6 — TGA-DTA curves of coumarine doped GLS crystal.

Table 4 — HOMO-LUMO energy gap and related molecular properties of coumarin doped glycene lithium sulphate.

Molecular properties	B3LYP/6-311+G(d,p)
HOMO	-0.2030
LUMO	-0.0245
Energy gap	-0.1785
Ionisation potential (I)	0.2030
Electron affinity (A)	0.0245
Global softness (s)	11.2044
Global hardness (η)	0.08925
Chemical potential (μ)	-0.11384
Global electrophilicity (ω)	0.0725

determined by B3LYP/6–311+G(d,p) method and listed in Table 5. The Figs 7-9 depicts the correlation of entropy (*S*), heat capacity at constant pressure (*C*p) and enthalpy change ($\Delta H0 \rightarrow T$) with temperature along with the correlation equations. From Table 9, one can find that the entropies, heat capacities, and enthalpy changes are increasing with temperature ranging from 100 to 1000 K due to the fact that the molecular vibrational intensities increase with temperature[25]. These observed relations of the thermodynamic functions versus temperatures were fitted by quadratic formulas, and the corresponding fitting regression factors (R_2) are all not less than 0.9995. The corresponding fitting equations for Coumarin doped Glycene Lithium Sulphate are:

$$S = 230.41 + 0.5\,T - 11.608 \times 10^{-4}\,T^2$$
$$Cp = 52.242 + 0.179\,T - 11.715 \times 10^{-4}\,T^2$$
$$\Delta H = -22.982 + 0.160\,T + 6.934 \times 10^{-4}\,T^2$$

3.9 Mulliken population analysis

The charge distributions calculated by the Mulliken method for the equilibrium geometry of Coumarin doped Glycene Lithium Sulphate with DFT/6-311+G(d,p) are listed in Table 6. The charge distribution on the molecule has an important influence on the vibrational spectra. The corresponding Mulliken's plot is shown in Fig. 10. From the results it is clear that the substitution of C-O atoms in the aromatic ring leads to a redistribution of electron density. The σ-electron withdrawing character of the chlorine atom in this title compound is demonstrated by the decrease of electron density on

Table 5 — Thermodynamic properties of coumarin doped glycene lithium sulphate determined at different temperatures with B3LYP/6-311+G(d,p) level.

T (K)	*S* (J/mol.K)	*C*p (J/mol.K)	$\Delta H0 \rightarrow T$ (kJ/mol)
100	247.69	49.09	3.74
200.00	292.91	84.75	10.47
298.15	332.38	114.01	20.26
300.00	333.08	114.51	20.47
400.00	369.54	139.38	33.21
500.00	402.91	159.68	48.20
600.00	433.51	175.92	65.01
700.00	461.64	188.95	83.27
800.00	487.59	199.60	102.72
900.00	511.63	208.52	123.14
1000.00	534.01	216.13	144.38

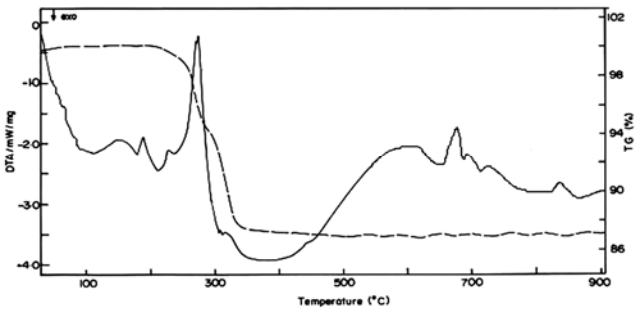

Fig. 6 — TGA-DTA curves of coumarine doped GLS crystal.

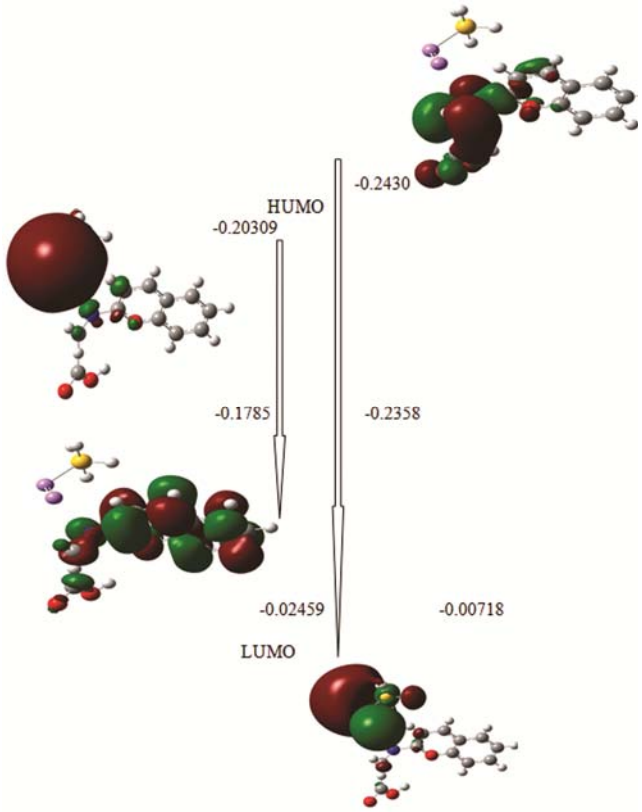

Fig. 7 — Frontier orbital energy of coumarin doped glycene lithium sulphate.

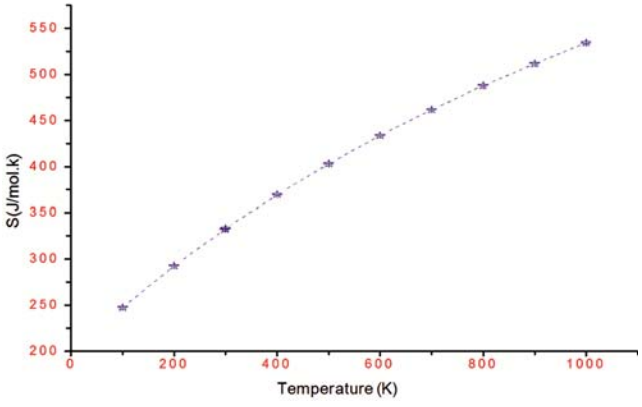

Fig. 8 — The effect of temperature on entropy (*S*) of coumarin doped glycene lithium sulphate.

Table 6 — The charge distribution calculated by the Mulliken atomic charges method for coumarin doped glycene lithium sulphate DFT/6-311++(d,p) basis set.

Atoms	B3LYP/6-311+G(d,p)
C1	-0.094848
C2	-0.165242
C3	-0.037782
C4	0.064479
C5	-0.094767
H6	-0.138847
C7	0.133699
C8	0.064479
H9	-0.037782
C10	-0.165242
C11	-0.094848
C12	-0.138847
H13	-0.094767
H14	0.173397
H15	0.131973
O16	-0.318240
N17	-0.495232
H18	0.083890
H19	0.083890
H20	0.130662
C21	0.127852
O22	-0.685051
O23	-0.699772
O24	0.130662
Li25	0.127852
Li26	0.222823
S27	0.485407
H28	0.131973
H29	0.585277
H30	0.173397
H31	0.287984

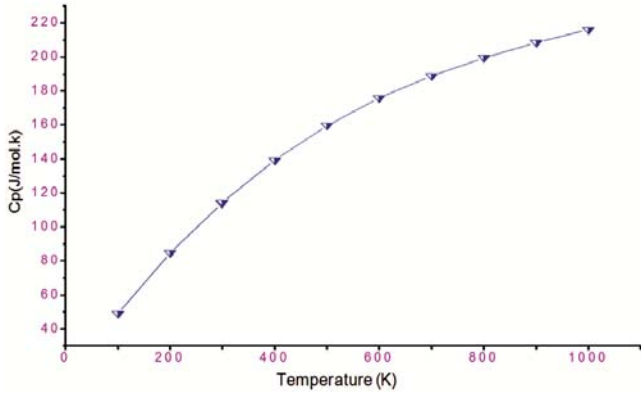

Fig. 9 — The effect of temperature on heat capacity (C_p) of coumarin doped glycene lithium sulphate.

O_{22} atom. The atomic charges in the S group are almost identical. The atomic charges obtained from 6-311+G(d,p) basis set shows that C_7 atom is more acidic due to more positive charge whereas H are more negative (Table 6).

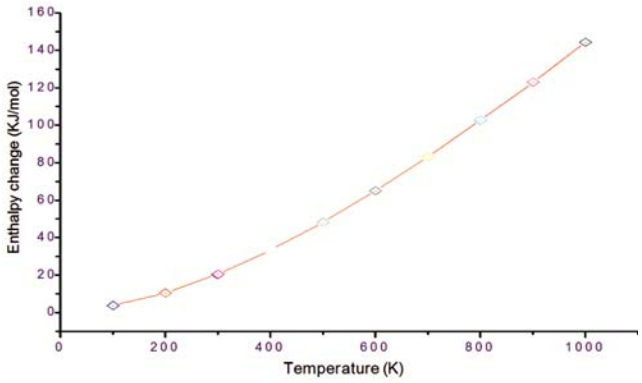

Fig. 10 — The effect of temperature on enthalpy change ($\Delta H0 \rightarrow T$) of coumarin doped glycene lithium sulphate.

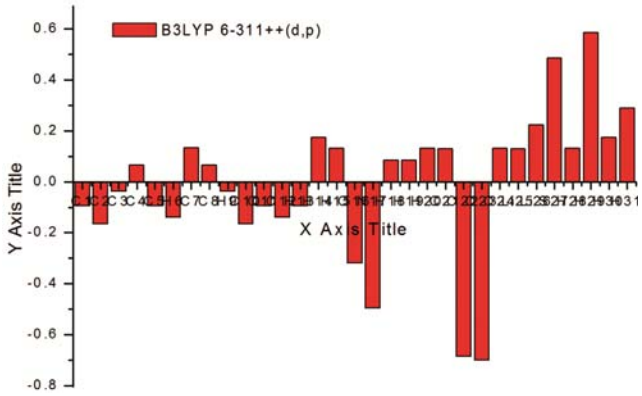

Fig. 11 — Mulliken plot of coumarin doped glycene lithium sulphate.

4 Results and Discussion

X-ray diffraction studies have been carried out to confirm the crystallinity and to calculate the lattice parameters of the grown samples. Using the monoclinic crystallographic equation, the lattice parameter values of doped GLS crystals were calculated and compared with the literature values. This confirms that the doped GLS single crystal retain its own crystal system [26]. The TG curve of this sample indicates that the sample is stable up to 210 °C and above this temperature the weight loss occurred due to self-degradation of doped GLS but merely to its evaporation after its melting. Three prominent and interesting features of ferroelectrics of doped GLS crystals are their reversible polarization, anomalous behavior (optical, thermal, elastic, etc.) and their non-linearities[27]. The ferroelectric materials cease to be ferroelectric above a certain temperature, known as transition temperature and show normal dielectric behavior. At the transition temperature the dye doped GLS crystal undergoes a transition from ferroelectric phase to a high symmetry phase and permittivity

increases sharply to a very high value which was referred to be anomalous in the neighborhood. The highest symmetry phase compatible with the ferroelectric structure is termed as the prototype phase also called paraelectric phase. Although it is not necessary of non-polar character, it was proves to be the greatest majority of known ferroelectrics so far. Most of the phases actually exist as the highest temperature phase of the crystal, although in some instances the structure may melt before the prototype phase would otherwise become stable [28]. As a result of its small structural displacement from the prototype, a typical ferroelectric material possesses a spontaneous polarization P_s which decreases with the increase of temperature T_c.

5 Conclusions

Good optical quality single crystals of Coumarin dye doped GLS have been grown from solution by slow solvent evaporation technique for the first time. Experiments were allowed to run for considerably larger duration of the time (20 days) can grow large crystals. The functional groups present in the grown crystals have been confirmed by FT-IR spectral analysis. The observed frequencies were assigned on the basis of symmetry operation on the molecule and normal coordinate analysis. The crystallinity of the grown sample was confirmed by single crystal X-ray diffraction analysis. Thermal stability of the grown sample was studied by TG and DTA analysis. The results from TG and DTA studies dye doped GLS crystals were stable up to 210 °C. The exothermic peak at 290 °C indicates a phase change from liquid to vapour state as evident from the loss of weight of about 87% in TG curve. Optical transmission UV-Visible spectral) range of dye doped GLS was measured and the doped GLS crystal has a good optical transmission in the entire visible region. The powder SHG measurement shows that the grown doped GLS crystal has 1.65 times higher SHG efficiency than KDP. Vickers micro hardness was calculated in order to understand the mechanical stability of the grown crystals. Each type of constituent chemical bond is regarded as one part of the whole crystal that has contributions to the total nonlinearity. The distribution of valence electrons of the metallic elements is an important factor that strongly affects the linear and nonlinear properties of each type of constituent chemical bond. The fundamental beam of 1064 nm from Q-switched Nd:YAG laser was used to test the SHG property of the grown crystal. The non-linear response of the physical properties with respect to the electric field and temperature is a unique characteristic of ferroelectric materials. This makes them extremely attractive materials for a variety of applications, particularly based on their anomalous electrical and optical properties. These sites give information about the region from where the compound can undergo non-covalent interaction. HOMO, LUMO, and Mulliken was calculated and compared with the experimental data. Finally, the thermodynamic properties to the title compound have been calculated for different temperatures, revealing the correlations among ((Cp), (S) and ($\Delta H0 \rightarrow T$)) and temperatures are obtained.

Acknowledgement

We gratefully acknowledge financial supports from the Department of Science & Technology-Science and Engineering Research Board [DST-SERB-FAST TRACK, PS-20/2009(SR)], New Delhi, India.

References

1 Hoshino S, Okaya Y & Pepinsky R, *Phys Rev*, 115 (1959) 1955.
2 Natarajan S, Ravikumar K & Rajan S S, *Kristallogr Z*, 168 (1984) 75.
3 Pepinsky R, Okaya Y, Eastman D P & Mitsui T, *Phys Rev*, 107 (1957) 1538.
4 Pepinsky R, Vedam K & Okaya Y, *Phys Rev*, 110 (1958) 1309.
5 Hoshino S, Mitsui T, Jona F & Pepinsky R, *Phys Rev*, 107 (1957) 125.
6 Ravikumar K & Rajan S S, *Kristallogr Z*, 171 (1985) 201.
7 Natarajan S & Mohan R J K, *Kristallogr Z*, 152 (1984) 179.
8 Baran J, Drozd M, Pietraszko A, Trzebiatowska M & Ratajczak H, *Polish J Chem*, 77 (2003) 1561.
9 Deepthy A & Bhat H L, *J Cryst Growth*, 226 (2001) 287.
10 Narayan Bhat M & Dharmaprakash S M, *J Cryst Growth*, 235 (2002) 511.
11 Narayanan P & Venkataraman S, *Kristallogr Z*, 142 (1975) 52.
12 Nagaraja H S, Upadhyaya V, Mohan Rao P, Aithal S & Bhat A P, *J Cryst Growth*, 193 (1998) 674.
13 Chakraborty D & Manogaram S, *Chem Phys Lett*, 294 (1998) 56.
14 Krishnakumar R V, Subha N M, Natarajan S, Sivakumar K & Vaghese B, *Acta Crystallogr C*, 57 (2001) 1149.
15 Fleck M & Bohaty L, *Acta Crystallogr C*, 60 (2004) 291.
16 Balakrishnan T & Ramamurthi K, *Cryst Res Technol*, 41 (2006) 1184.
17 Narayana M B, Jayarama A, Sureshkumar M R & Dharmaprakash M S, *J Cryst Growth*, 280 (2005) 581.
18 Krishnakumar V & Nagalakshmi R, *Spectrochim Acta A*, 61 (2005) 499.
19 Ge W, Zhang H, Wang J, Ran D, Sun S, Xia H, Liu J, Xu X, Hu X & Jiyang M, *J Cryst Growth*, 282 (2005) 320.
20 Vijayan N, Rajasekaran S, Bhagavannarayana G, Rameshbabu R, Gopalakrishnan R, Palanichammy M & Ramasamy P, *Cryst Growth Des*, 6 (2006) 2441.

21 Wellen R M R & Rabello M S, *J Mater Sci*, 40 (2005) 6099.
22 Selvaraju K, Kirubavathi K, Vijayan N & Kumararaman S, *J Cryst Growth*, 310 (2008) 2859.
23 Sambathkumar K & Nithiyanantham S, *J Mater Sci: Mater Electron*, 28 (2017) 6529.
24 Cecily M G D, Sambathkumar K, Madivanane R, Velmurugan G, Gayathri R, Nithiyanantham S, Venkatachalapathy M & Rajkamal N, *J Mol Struct*, 1163 (2018) 480.
25 Cecily M G D, Madivanane R & Sambathkumar K, *Indian J Pure Appl Phys*, 55 (2017) 638.
26 Sankar R, Ragahvan C M, Mohan K R & Jayavel R, *J Cryst Growth*, 309 (2007) 3036.
27 Hobza P & Havlas Z, *Chem Rev*, 100 (2000) 4253.
28 Jayalashami K, Sridhar M A, Shashidhara P J, Naraayan B M & Gharamprakash S M, *Mol Cryst Liq Cryst*, 393 (2003) 99.